CHAPTER 7

SEDIMENT TRANSPORT AND BEACH PROFILE CHANGE DUE TO RANDOM WAVES

SHINJI SATO
University of Tokyo
Tokyo, Japan

1. INTRODUCTION

Beach erosion has been a serious problem in the past several decades. It has been especially significant in recent years as a consequence of reduction of sand supply from rivers following reservoir construction and dredging of submarine sand and minerals. Increasing needs for utilization of coastal zones and the construction of port facilities also block the littoral drift, resulting in severe erosion on the down-drift side and excessive accretion on the up-drift side. According to Bird [6], more than 70% of sandy coasts around the world are categorized as eroding beaches. The recent trend of sea level rise due to global warming may accelerate the erosion. In order to find effective countermeasures against beach erosion, we have to understand the mechanism of sediment transport in detail. However, our knowledge of sand transport mechanisms on natural beaches is still qualitative, which sometimes forces us to rely on experience.

In order to predict beach evolution quantitatively, we have to understand first the dynamics of waves and currents in nearshore environments. Waves in nature are, however, random and sediment transport mechanisms under random waves are complex. Laboratory experiments in wave flumes have been used as powerful techniques to investigate the mechanisms under well-controlled environments. A number of valuable data on the mechanics of the wave boundary layer, incipient motion of sand particles, and suspended sand concentration above sand ripples have been accumulated by laboratory measurements using monochromatic waves. However, they may not be used directly to explain sediment transport in nature owing to the presence of scale effects and wave randomness. Large wave flumes equipped with random wave generators and oscillatory flow tanks have been constructed during the last decade, making possible the study of sediment transport mechanisms with quasiprototype scales. Field investigations and numerical modeling have also been performed extensively with new measuring instruments and computer facilities.

In this chapter, recent progress in the field of coastal dynamics under random waves is reviewed. The role of long-wave components in the coastal dynamics and numerical modeling under random waves is described in detail. Sand transport in nearshore areas is usually treated as longshore transport and cross-shore transport. Longshore transport is considered to be significant in long-term beach evolution, whereas cross-shore transport is considered to be responsible for short-term or seasonal variation. Both types of transport are affected by wave randomness; frequency spectrums are more associated with cross-shore sediment movement and longshore transport is more associated with directional spectrums. Long waves of the trapped and leaky modes may also affect both cross-shore and longshore transport, playing a significant role in the formation of three-dimensional rhythmic topographies. As longshore transport was reviewed in detail by Komar [17], this chapter will concentrate on cross-shore transport mechanisms and resulting beach profile changes under random waves.

2. CLASSIFICATION OF BEACH PROFILES

It is widely accepted that beach profiles are classified as summer (accretive) profile and winter (erosional) profile (e.g., Komar [16], Horikawa [11]). The conditions determining which type will be developed have been studied by Johnson [13], Saville [35], and Iwagaki and Noda [12]. Several parameters, including offshore wave steepness, sediment grain size, and bed slope, have been identified as essential.

Dean [9] introduced the following parameters to determine the resultant beach profile types:

$$C_1 = \left(\frac{H_0}{L_0}\right)\left(\frac{\pi w_s}{gT}\right)^{-1} \tag{1}$$

$$C_2 = \frac{H_0}{w_s T} \tag{2}$$

where H_0 is the deep-water wave height, L_0 the deep-water wavelength, w_s the settling velocity of sand particle, T the wave period, and g the gravity acceleration. Dean [9] showed that the erosional beach profile developed for $C_1 > 1.7$ or $C_2 > 0.85$ and the accretive profile developed otherwise.

Kriebel et al. [19] carried out small-scale laboratory experiments to verify whether

small-scale experiments are capable of reproducing prototype scale experiments. The sediment size in the small-scale model was determined so that the undistorted Froude model had the same C_2 value as the prototype scale experiments. They concluded that the beach profiles under the undistorted model were similar to those under prototype scale experiments and that the beach profiles in small-scale experiments and prototype experiments can be classified by the same C_1 or C_2 values, although the critical values they found were different from those originally proposed by Dean [9]. They suggested the difference is due to the scale effects incorporated in Dean's original criteria.

Kraus et al. [18] evaluated the applicability of various criteria on the basis of laboratory data in large wave tanks using monochromatic waves and field data. They examined the classification of beach profiles by the combination of various nondimensional parameters, including C_1 and C_2, and concluded that simple criteria successfully predict the beach profiles for both large wave tank data using monochromatic waves and field data using random waves if the mean wave height was used in the field application.

Sunamura and Horikawa [41] classified the beach profiles into three types—erosional, accretive, and the intermediate—and showed that the development of each type was dependent on the following C_3 value:

$$C_3 = \left(\frac{H_0}{L_0}\right)\left(\frac{D}{L_0}\right)^{-0.67}(\tan\beta)^{0.27} \tag{3}$$

where D is the sediment grain size and $\tan\beta$ the initial beach slope. They showed that beach profiles change from accretive to intermediate and intermediate to erosional as C_3 increases, and found the boundary C_3 values to be 4 and 7, respectively, for the condition of laboratory monochromatic waves. The boundaries were 9 and 18 for field data, where significant wave height was used to calculate C_3.

Mimura et al. [22] performed a series of small-scale laboratory experiments to study beach profile change due to random waves. Figure 7.1 is the classification of beach

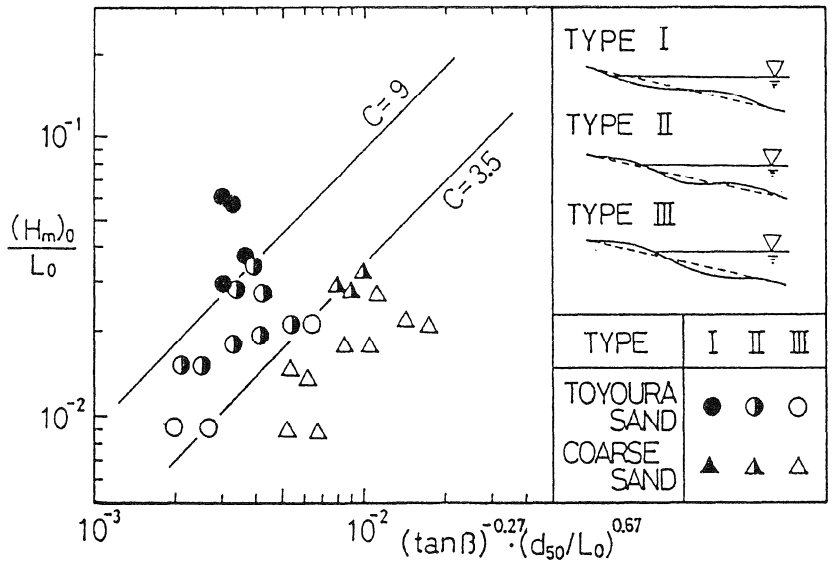

FIGURE 7.1. Classification of beach profiles for random waves in a laboratory flume [22].

profiles. Circular symbols are for 0.18 mm fine sand (Toyoura sand in the figure) and triangles are for 0.75 mm coarse sand. Mimura et al. [22] found that the boundary between accretive and intermediate profiles was expressed by $C_3 = 3.5$ and that between intermediate and erosional profiles by $C_3 = 9$ when the C_3 value was estimated on the basis of mean wave height. When the significant wave was used instead of the mean wave, the critical values of C_3 changed from 3.5 to 5 and 9 to 13, respectively. The correspondence between the boundary C_3 laboratory data values obtained with random waves and those obtained with monochromatic waves is better when the mean wave height is used, which agrees with the conclusion of Kraus et al. [18]. The difference between the boundary C_3 laboratory data values ($C_3 = 5$ and 13) obtained by random waves and those obtained by field data ($C_3 = 9$ and 18) is considered to be due to the scale effect and three-dimensionality in the field.

The use of simple criteria to determine beach profile types is thus found to be promising even for the condition of random waves to understand the macroscopic trend of beach profile change. However, in order to predict the dynamic response of beach profiles to variable sea states, more sophisticated models based on the physical processes of local sand transport are required.

Mimura et al. [22] also observed that beach transformation under random waves is different from that under monochromatic waves as follows:

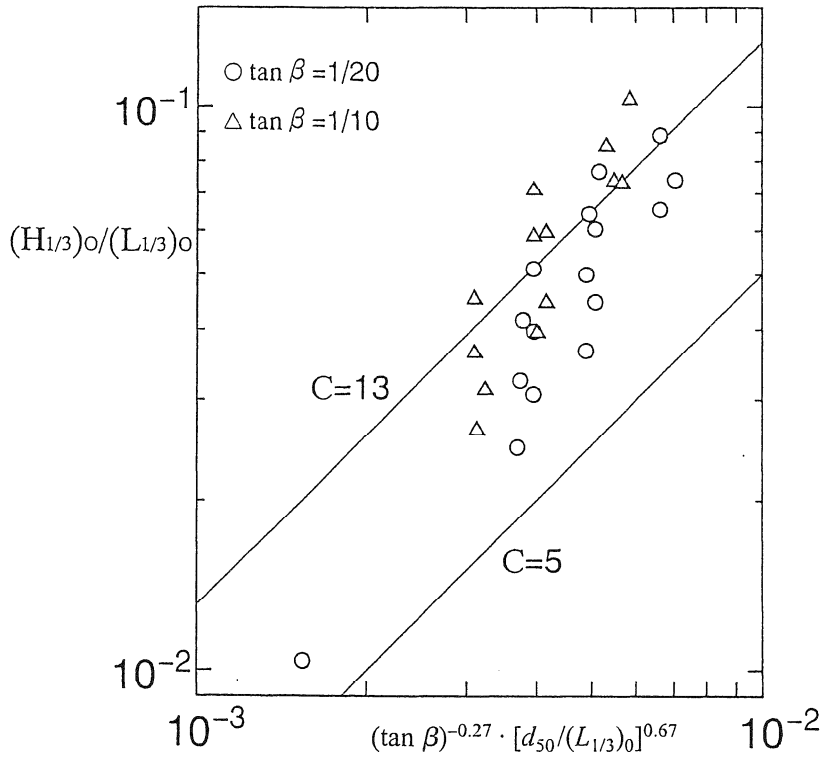

FIGURE 7.2. Classification of beach profiles for bichromatic grouping waves in a laboratory flume.

1. Intermediate beach profiles are more frequently developed
2. The speed of beach deformation is slower

These differences are considered to be closely associated with characteristics of randomly breaking waves. The variation in breaking points will directly affect the locations of sand suspension and the process of bar formation in the outer surf zone, and consequently affect the sediment transport in the inner surf zone since it influences the development of long waves and undertow.

Effects of the variation in breaking points and the development of long waves on cross-shore sediment movement can also be investigated in laboratory experiments by using bichromatic grouping waves. Figure 7.2 shows the classification of beach profiles due to bichromatic grouping waves in laboratory experiments, where the second-order Stokes wave theory was used to generate the incident wave. In all runs of experiments shown in Figure 7.2, the resultant beach profiles were of the intermediate type, even for large C_3 values, indicating that the intermediate beach profiles are more dominant under grouping waves than random waves. This suggests that the long wave, which is more pronounced in grouping waves, tends to contribute to the berm formation near the shoreline.

3. NEAR-BOTTOM VELOCITIES UNDER RANDOM WAVES

3.1. Asymmetry in Velocity Variation

The estimation of near-bottom velocity is important, since it provides fundamental information on sand transport mechanisms. The near-bottom velocity u of random waves involves fluctuation over a wide range of frequencies and is expressed as follows:

$$u = U + u_w + u_l + u_t \tag{4}$$

where U is steady current component or undertow, u_w the short-wave components originally dominated in the incident wave spectrum, u_l the long-wave components incident as free waves and/or induced through the nonlinear interaction of short-wave components, and u_t turbulence generated by wave breaking as well as that generated in the bottom boundary layer. The onshore velocity is defined to be positive in this chapter. In order to predict the velocity variation with good accuracy, proper modeling for each component is required.

In oscillatory flow tank tests using asymmetric oscillations, Sato and Horikawa [32] and Ribberink and Al-Salem [28] confirmed that the net sand transport rate was closely correlated with the velocity amplitude as well as the asymmetry in velocity variations. The asymmetry in velocity variation under shallow-water waves is realized in various ways, as shown in Figure 7.3. Undertow itself is considered to be an asymmetry superimposing a bias in near-bottom velocities. Wave nonlinearity will produce a skewed variation with sharp crest and flat trough at short-wave velocities. Wave nonlinearity will also tend to tilt the wave in the surf zone, producing asymmetry in the acceleration. Phase-dependency of long waves on the short-wave envelope will produce other type of asymmetry, which will influence the slowly varying transport of sediments. Turbulence may induce another asymmetry when it has a specific phase-dependency on wave-orbital velocities. These asymmetries are mixed together on natural beaches and influence sand transport in various manners. It is considered, for example, that the asymmetry in short-

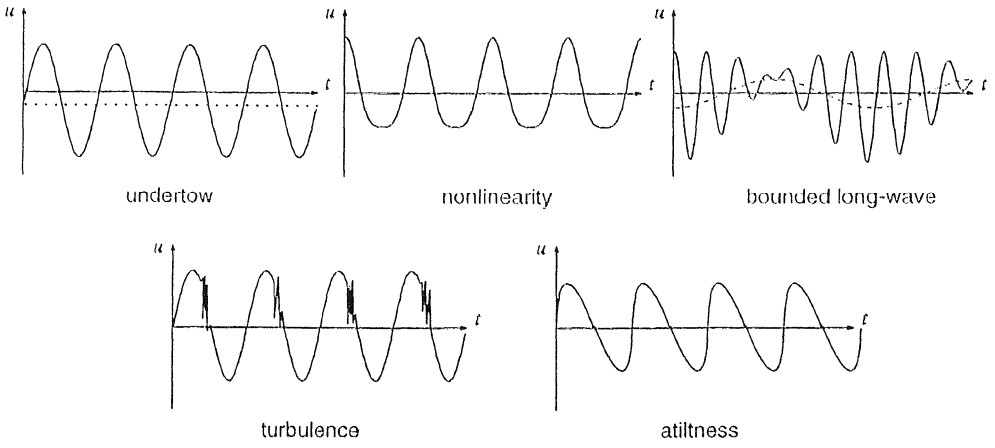

FIGURE 7.3. Various asymmetry in velocity variation.

wave components will primarily influence sediment transport near the bed, whereas the asymmetry due to bound long waves and turbulence will influence the transport of suspended sediment.

Many models have been presented to estimate near-bottom velocities under random waves. The first model to be established was the model that simulates the transformation of short waves due to random wave breaking. Undertow and long-wave components are consequently modeled on the basis of the short-wave computation. The estimates of u_w, U, and u_l are briefly described herein. Turbulence will not be discussed in this chapter, since the definition of turbulence in random wave fields is still uncertain, although it plays an important role in sand suspension. It should be noted here that nonlinear wave models were also used recently in beach evolution modeling, in which long wave and steady components were solved simultaneously with short-wave computation [34].

3.2. Short Waves

Many models have been proposed to estimate velocity variation due to short-wave component both in the frequency domain and in the physical domain [3]. In the frequency domain, the amplitude $\hat{u}_w(f)$ of near-bottom velocity variation under random waves is related to the amplitude $\hat{\eta}(f)$ of surface elevation as

$$\hat{u}_w(f) = \frac{2\pi f}{\sinh kh}\hat{\eta}(f) \tag{5}$$

where k is the wave number at frequency f and h is the water depth. Since Equation 5 is based on the linear wave theory, no asymmetry is involved in the simulated velocity variation as long as the surface elevation is simulated as a sum of sinusoidal waves. In order to simulate asymmetric velocities, the interaction of each wave component should be incorporated. Sato and Horikawa [32] applied the second-order Stokes wave theory to the estimation of asymmetric near-bottom velocity under random waves. However, the application is limited to nonbreaking waves in relatively deep water.

Models in the physical domain have been more frequently used in beach evolution modeling since they can more easily incorporate the wave-height decay due to wave

breaking in surf zone. In the physical domain models, the cross-shore distribution of short-wave heights in surf zone was computed by introducing heuristic wave decay models [31, 39] or was computed numerically on the basis of depth-integrated mass and momentum equations [45, 33]. The asymmetry in near-bottom velocity was then introduced with various nonlinear wave theories, such as stream-function theory [31], cnoidal wave theory [33], and vocoidal theory [39]. In a recent model based on the Boussinesq equation, asymmetric velocity variations were simulated directly [34].

The asymmetry in velocity due to short waves is likely to produce net onshore transport, since more sand will be transported shoreward by larger onshore velocity under the wave crest. However, the direction will be reversed for the transport of fine sand above rippled beds [32].

3.3. Undertow

Undertow is breaking-induced, offshore-directed flow below trough level that compensates onshore mass flux near the surface due to the propagation of breaking bores. The estimation of undertow is important in modeling offshore transport [7, 40]. Although sophisticated models predict the vertical profile of undertow velocity on the basis of eddy viscosity assumptions [43, 25], the undertow velocity near the bottom is the most important in sand transport modeling, since suspended sand concentration becomes exponentially large near the bottom.

The steady component U of near-bottom velocity can be computed as a compensating return flow of onshore mass flux due to breaking bores. When we assume that the cross-sectional area of a breaking bore is proportional to the square of wave height and that the compensating flow is uniform over the water depth, we can roughly estimate the steady velocity U by

$$U = -A\frac{H^2}{dT} \tag{6}$$

where H is the local wave height, d the mean water depth, and T the wave period. The coefficient A was determined to be 4 on the basis of laboratory data for monochromatic waves [33]. The steady velocity under random waves can be estimated from the sum of mass fluxes due to individual breaking waves. For random waves, H^2 in Equation 6 is replaced by the sum of H^2 of breaking waves, while T is replaced by the sum of all wave periods. Figure 7.4 shows a comparison of undertow velocity under random waves. In spite of rough assumptions introduced, the model reproduces the cross-shore distribution of undertow quite accurately. It should be noted here that wave randomness tends to smooth out various discontinuities at the breaking point of monochromatic waves. The estimation of undertow by Equation 6 is a typical example; it predicts a large gap at the breaking point for monochromatic waves but with rather smooth distribution, as in Figure 7.4 for random waves.

3.4. Long Waves

Long waves or infragravity waves, with periods several times as long as short waves, become pronounced as they increase their heights near the shoreline, where short waves decrease their heights owing to the energy dissipation due to wave breaking. Mechanisms of

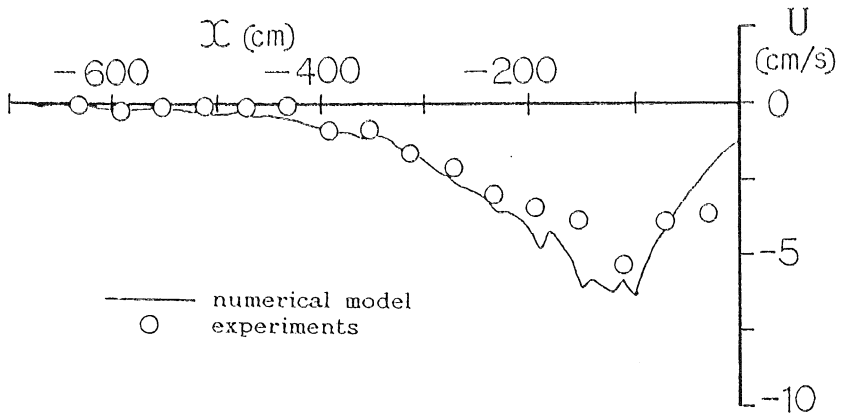

FIGURE 7.4. Distribution of undertow velocity [33].

the development of long waves have been investigated by many researchers [44, 21, 23]. Three major mechanisms are suggested:

1. Incidence of free long waves
2. Temporal variation of set-up due to time-varying breaking point
3. Transition of the bounded long wave to free wave as a result of breaking of large waves in wave groups

The second and third mechanisms are associated with the grouped nature of the incident wave and can be modeled by the long-wave equation with a radiation stress term as a forcing term [33, 29]. Governing equations for simulating the development of the long-wave component are

$$\frac{\partial \eta_l}{\partial t} + \frac{\partial}{\partial x}(u_l d) = 0 \tag{7}$$

$$\frac{\partial u_l}{\partial t} + u_l \frac{\partial u_l}{\partial x} + \frac{1}{\rho d}\frac{\partial S_{xxl}}{\partial x} = -g\frac{\partial \eta_l}{\partial x} - \frac{\tau_{xl}}{\rho d} \tag{8}$$

where ρ is the density of water, S_{xxl} the radiation stress, and τ_{xl} the bottom shear stress. The subscript l indicates that the term corresponds to the long-wave component. The radiation stress is estimated from the results of short-wave computation as

$$S_{xxl} = \rho g(\eta_w^2)_l\left(\frac{1}{2} + \frac{2kd}{\sinh 2kd}\right) \tag{9}$$

where η_w is the surface elevation due to the short-wave component and $(\eta_w^2)_l$ denotes the low-pass-filtered variation of η_w^2. The symbol k is the wave number for the significant wave computed by the linear theory. The bottom shear stress τ_{xl} can be computed by the following model proposed by Nishimura [24] for the wave-current field:

$$\tau_{xl} = \rho C_f(w + \hat{u}_w^2/w)u_l \tag{10}$$

$$w = (u_l + 2\hat{u}_w/\pi + |u_l - 2\hat{u}_w/\pi|)/2 \tag{11}$$

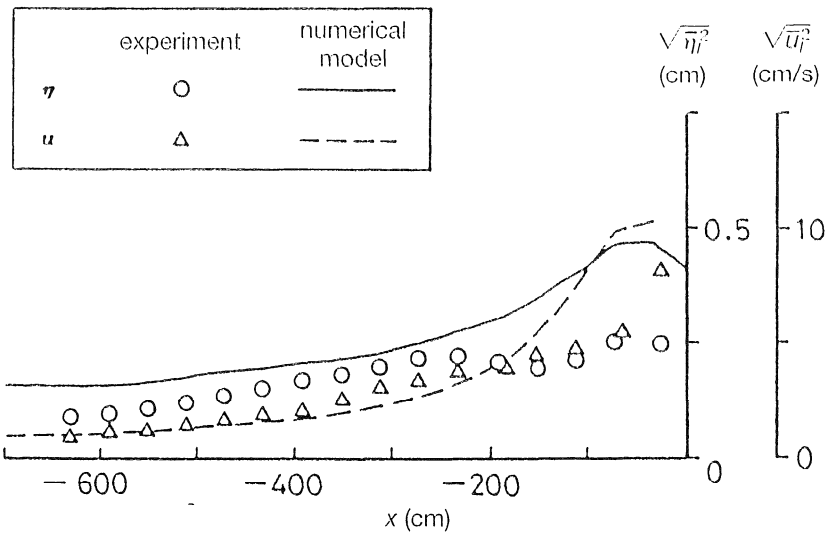

FIGURE 7.5. Development of long-wave component [33].

where C_f is the friction coefficient and $\hat{u}_w$ the amplitude of the near-bottom velocity due to the short-wave component.

The incident long wave at the offshore boundary can be estimated by the results of short-wave computation by

$$\eta_l = -\frac{S_{xxl}}{\rho(gd - C_g^2)} + \text{constant} \tag{12}$$

where the value of the constant is determined so that the mean water level of the incident wave train becomes zero.

Based on the results of short-wave computation, the development of the long-wave component can be estimated by the numerical integration of Equations 7 and 8. Figure 7.5 shows a comparison of cross-shore distributions of the root-mean-square amplitudes of η_l and u_l estimated on the basis of the model described in above. The development of the long-wave component towards the shoreline is simulated, although the model tends to overestimate the long wave in the vicinity of the shoreline. The phase-dependency of the simulated long wave on the short-wave envelope, which is essential in sediment transport, will be described in the next section.

4. EFFECTS OF LONG WAVES ON CROSS-SHORE SEDIMENT TRANSPORT

4.1. Suspended Sediment Flux

Effects of long waves on cross-shore sand transport have been studied. The oscillatory flow induced by long-wave components exert a greater influence on suspended loads than on bed loads. The contribution of long waves to suspended sand transport is evaluated by

the suspended sediment flux, expressed as the average of the product of instantaneous velocity and sediment concentration as follows:

$$\overline{uc} = \overline{UC} + \overline{u'c'} \tag{13}$$

where u and c are cross-shore velocity and suspended sand concentration, respectively, U and C are average time, and u' and c' are fluctuating components, respectively. The contribution $\overline{u'c'}$ of fluctuating components can be expressed as the sum of contributions from various frequencies. The relative contribution at different frequencies can be estimated by the cospectrum, cosp_{uc} between u and c, since it gives the cross-product between them as a function of frequency. The suspended sediment flux is therefore expressed by

$$\overline{uc} = \overline{UC} + \int_0^\infty \text{cosp}_{uc}\,df \tag{14}$$

Figure 7.6 shows a schematic diagram of suspended sand transport under bounded long waves. It was suggested by Shi and Larsen [36] that long waves bounded by wave groups would result in seaward transport. The mechanism is based on the reasonable assumption that c' is large under a series of large waves when u' is directed offshore. The sediment flux under large waves thus contributes significantly to seaward transport. As the velocity variation u' due to bounded long waves is directed onshore under small waves when c' is small, the net sand transport will be directed offshore. It should be noted, however, that the seaward transport is only realized by bounded long waves. As discussed in the previous section, long waves of various types are coexistent in nature, such as free incident waves, reflected waves from shoreline, and edge waves, which tend to obscure the seaward transport contributed by bounded long waves.

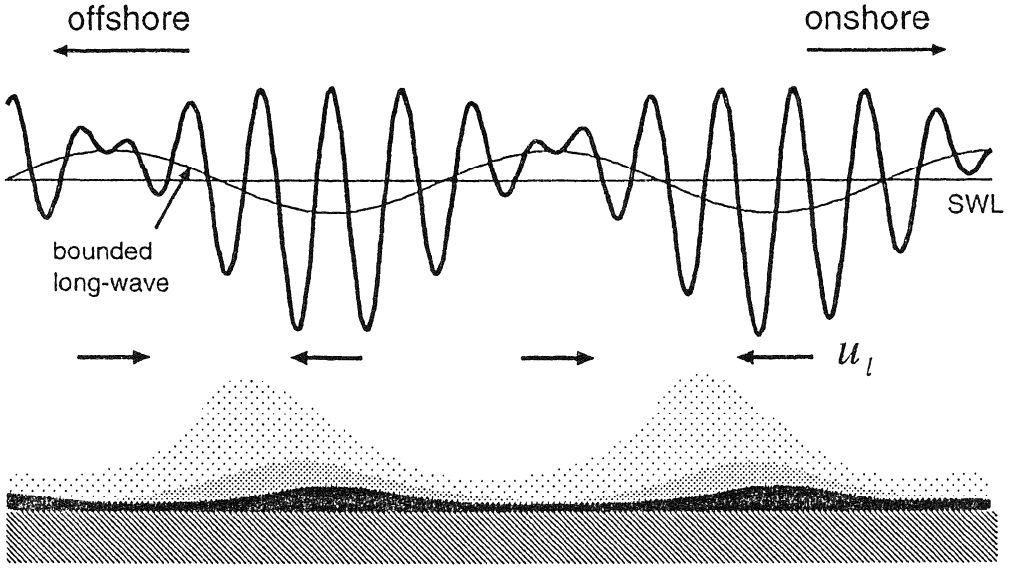

FIGURE 7.6. Schematic diagram of suspended sand transport under a bounded long wave.

4.2. Suspended Sediment Flux Offshore and Seaward of the Surf Zone

Sato and Horikawa [32] found on the basis of experiments with an oscillatory flow tunnel that the direction of sediment transport was determined by the asymmetry in velocity history. They simulated near-bottom velocity variations due to long-wave components by using the second-order Stokes wave theory. The simulated velocities showed the typical phase-dependency of long waves bounded to short-wave envelopes. Their data indicated that the net sand transport tended to be directed offshore as the relative magnitude of bounded long waves increased.

Figure 7.7 shows an example of field data obtained at the Ajigaura Coast facing the Pacific Ocean, Japan. The figure shows low-pass-filtered variations of near-bottom cross-shore velocity u_l (top), velocity squared $(u^2)_l$ (middle), and suspended sand concentration c_l (bottom) measured at 10 cm above the bottom near the breaking point. As the significant wave period was 8s, the long-wave component was extracted by using a numerical low-pass filter with cut-off frequency f_c of 0.033 Hz. It is apparent that the temporal variation of c_l is in phase with $(u^2)_l$, indicating that sand suspension was more pronounced under a series of large waves.

Figure 7.8 illustrates the joint probability density between u_l and $(u^2)_l$ and that between c_l and $(u^2)_l$ for the data shown in Figure 7.7. The bracket $< >$ implies that the variable was respectively normalized by the standard deviation. A strong positive correlation is noticed between suspended sand concentration c_l and wave energy level $(u^2)_l$ but the negative correlation between the cross-shore velocity u_l and wave energy level $(u^2)_l$ is less obvious. This indicates that only part of the long waves are bounded to the wave group and long waves generated by other mechanisms are also superimposed. Figure 7.9 shows the cospectrum between u and c. Suspended sediment transport due to the short-wave component is directed shoreward, while that due to long-wave component in a range 0.01 Hz $< f <$ 0.05 Hz is directed seaward, which suggests that bounded long waves are dominant in that frequency band.

The shoreward transport by short waves and the seaward transport by long waves were also reported by Osborne and Greenwood [26]. Figure 7.10 shows a cospectrum of the near-bed cross-shore velocity and suspended sand concentration observed seaward of the surf zone of a nonbarred shore face. The figure shows that short-wave components produce strong onshore transport at wind-wave frequencies ($0.1 < f < 0.5$ Hz), whereas long-wave components produce offshore transport at frequencies ($0 < f < 0.1$ Hz) lower than the wind-wave band. It should be noted however that the contribution of long waves is weak compared to the short-wave contribution. It is also noted that the contribution of long waves may be dependent on wave conditions. It may temporarily change its direction in swell-dominated waves and at various stages in a storm [46, 47].

4.3. Suspended Sediment Flux in the Surf Zone

Figure 7.11 shows the cospectra between u and c estimated in a random-wave experiment. In the experiment, cross-shore velocities and suspended sand concentration at 0.5 cm above bed were measured for the condition of random waves breaking on a 1/20 uniformly sloping bed filled with 0.2 mm sand. The dimension of the incident wave was $(H_0)_{1/3}$ = 11.7 cm and $T_{1/3}$ = 1.05 s. The value of x in Figure 7.11 denotes the distance from the still-water shoreline. The cospectrum at $x = -30$ cm, located in the vicinity of the shoreline, shows onshore-directed transport for the whole range of frequencies. The

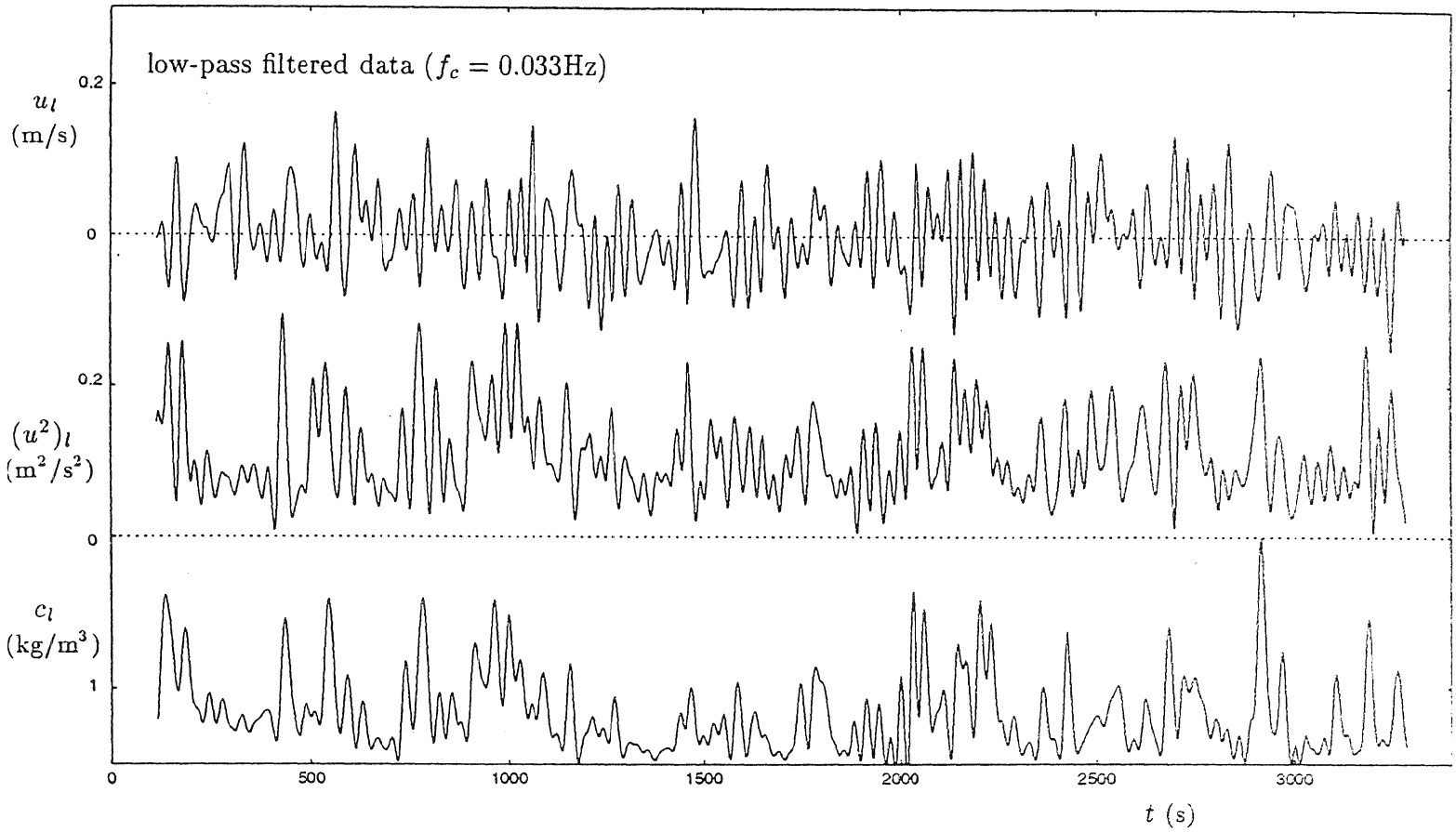

FIGURE 7.7. Low-pass-filtered variations of u, u^2, and c.

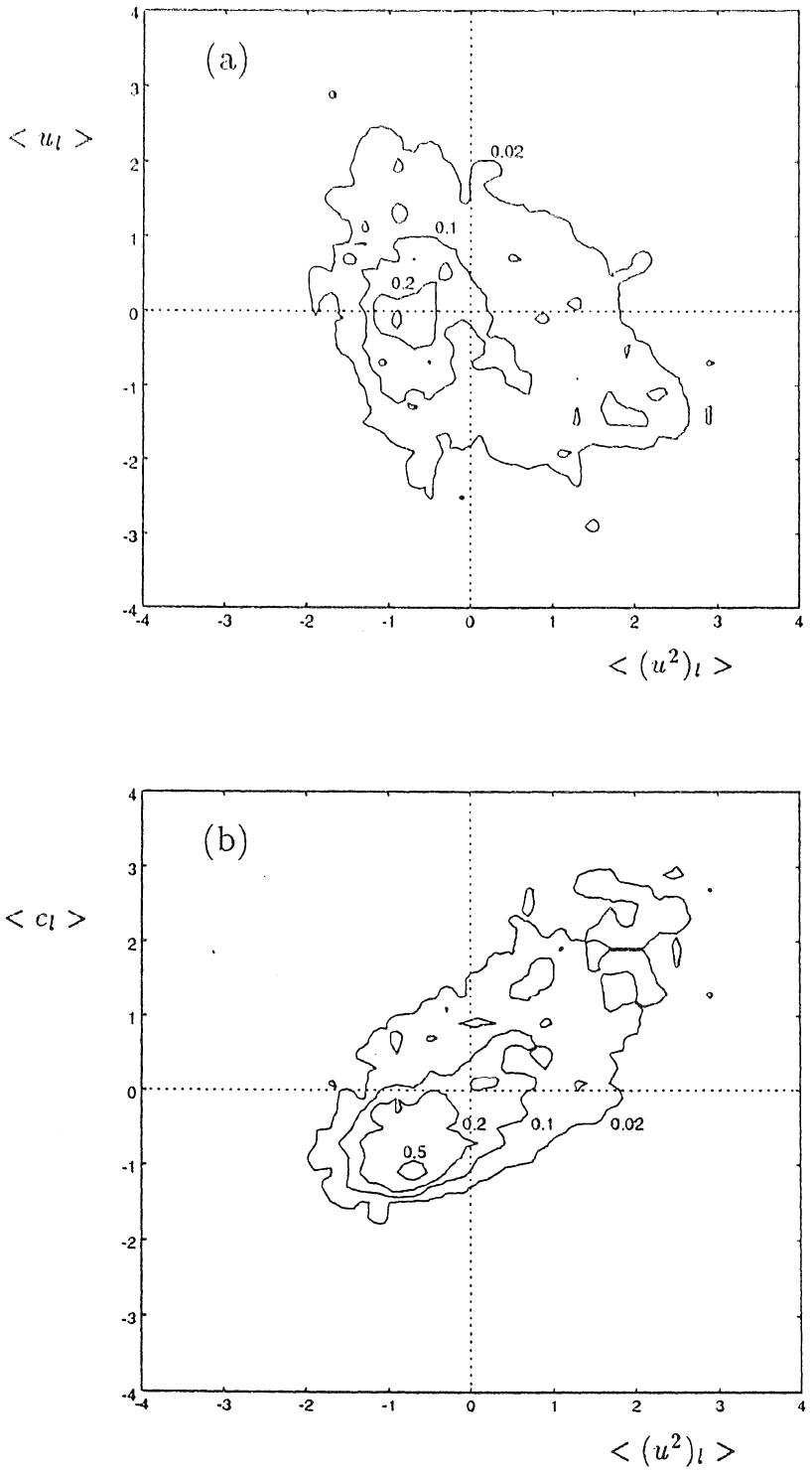

FIGURE 7.8. Probability density of u, u^2, and c.

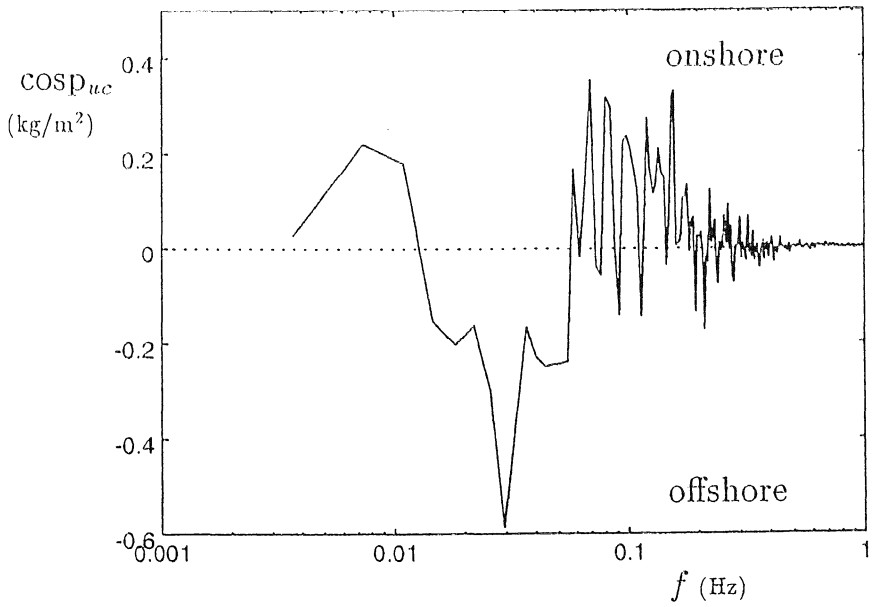

FIGURE 7.9. Cospectrum between u and c.

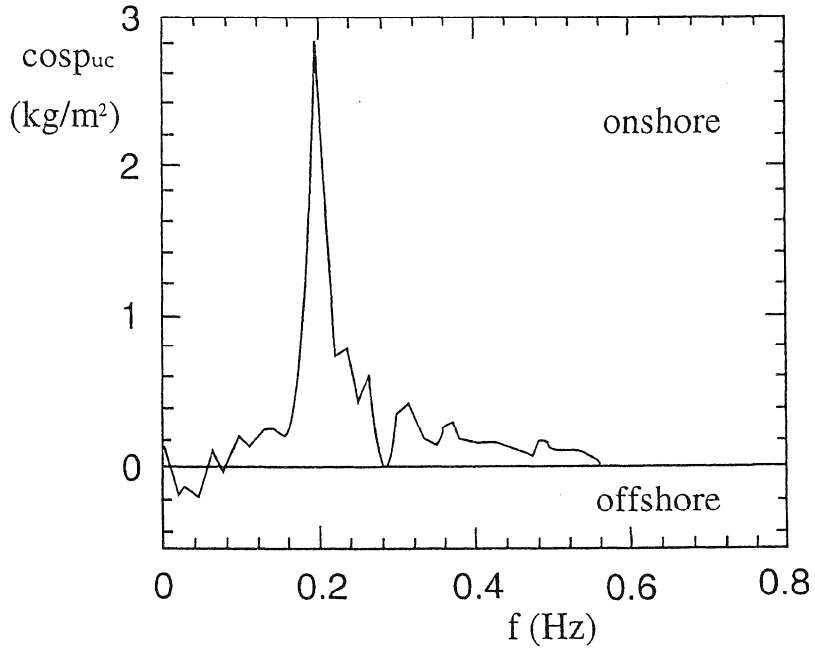

FIGURE 7.10. Co-spectrum between u and c [26].

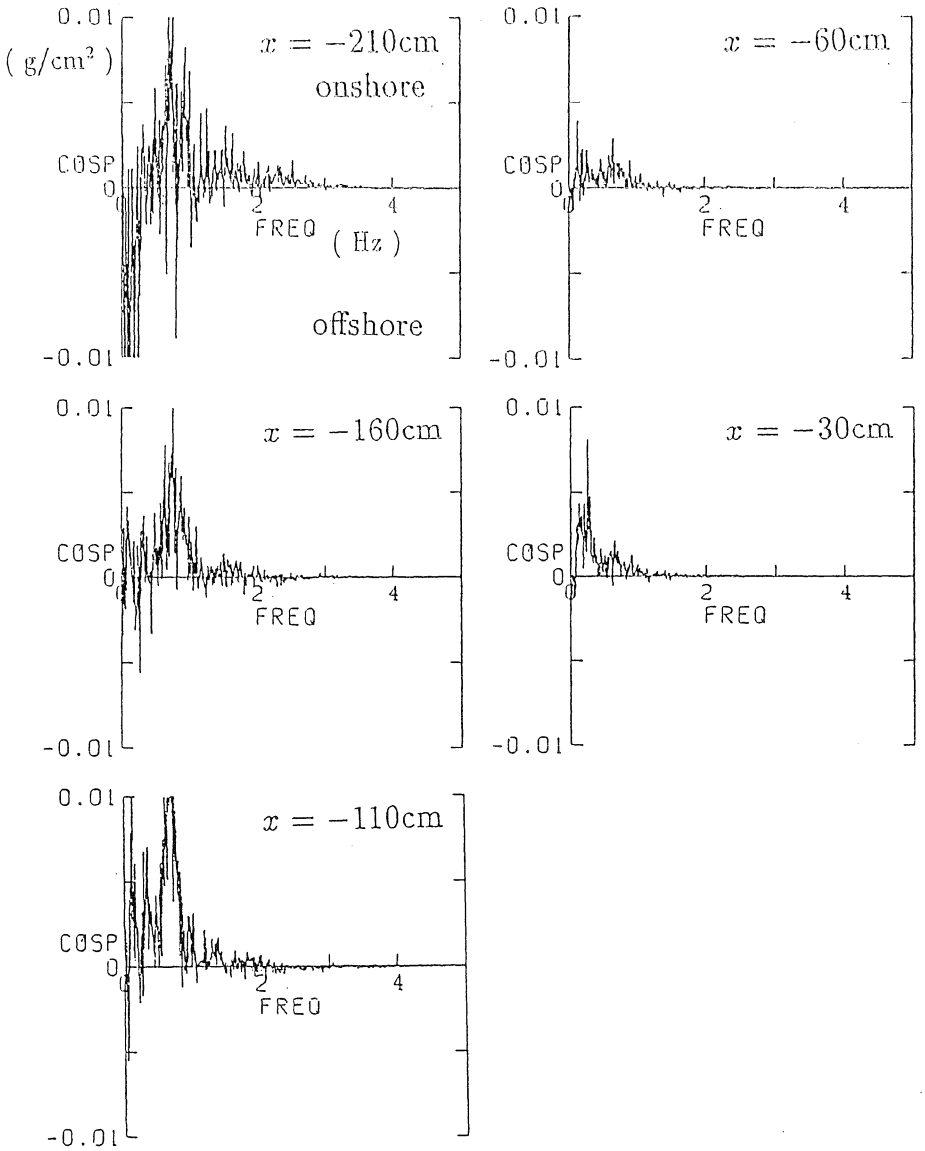

FIGURE 7.11. Cospectrum between u and c in a laboratory wave flume.

contribution by the long-wave component ($0 < f < 0.25$ Hz) is directed onshore near the shoreline but gradually tends to be directed offshore with increasing distance from the shoreline. The contribution of each frequency band to the total sediment flux is illustrated in Figure 7.12, in which the steady component is estimated by UC and the contributions of short waves $(uc)_w$ and long-waves $(uc)_l$ are respectively estimated by

$$(uc)_w = \int_{f_c}^{\infty} \mathrm{cosp}_{uc} df \tag{15}$$

$$(uc)_l = \int_{\infty}^{f_c} \mathrm{cosp}_{uc} df \tag{16}$$

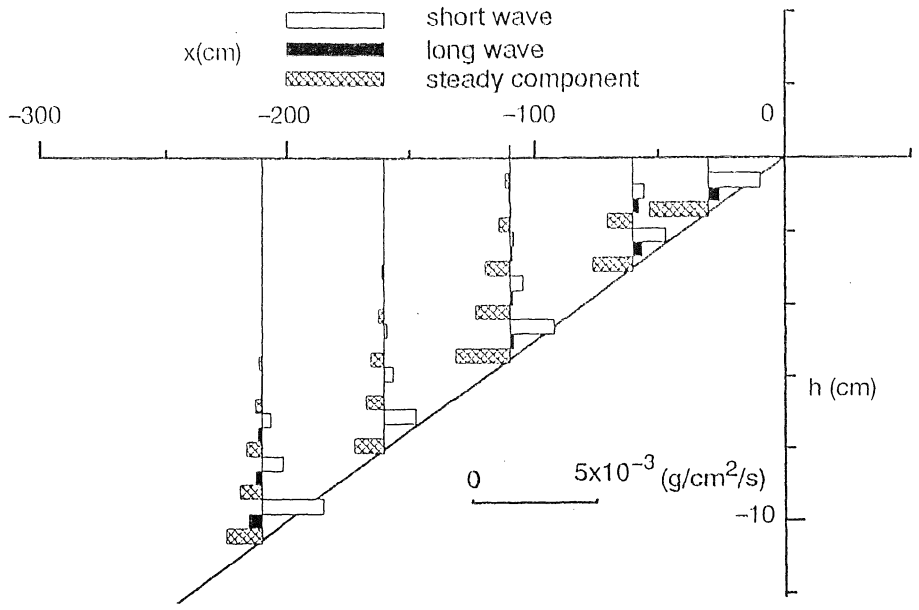

FIGURE 7.12. Contributions of various components to suspended sediment flux.

where f_c denotes the critical frequency between the long- and short-wave components, determined to be 0.25 Hz. Figure 7.12 indicates that the steady component, always directed offshore, demonstrates the largest contribution at all the points. The contribution of the short-wave components is always directed onshore and is almost as large as the contribution of the steady component. The contribution of the long-wave component is relatively small but directed offshore in the outer surf zone and onshore near the shoreline.

Beach and Steinberg [5] estimated the cospectra between u and c on the basis of field data obtained at the east and west coasts of the United States. Figure 7.13 shows cospectra for data obtained near the bottom of the outer surf zone (Figure 7.13a) and the inner surf zone (Figure 7.13b). The contribution of the long-wave component is directed offshore in the outer surf zone and onshore in the inner surf zone, which is consistent with laboratory measurements shown in Figure 7.11.

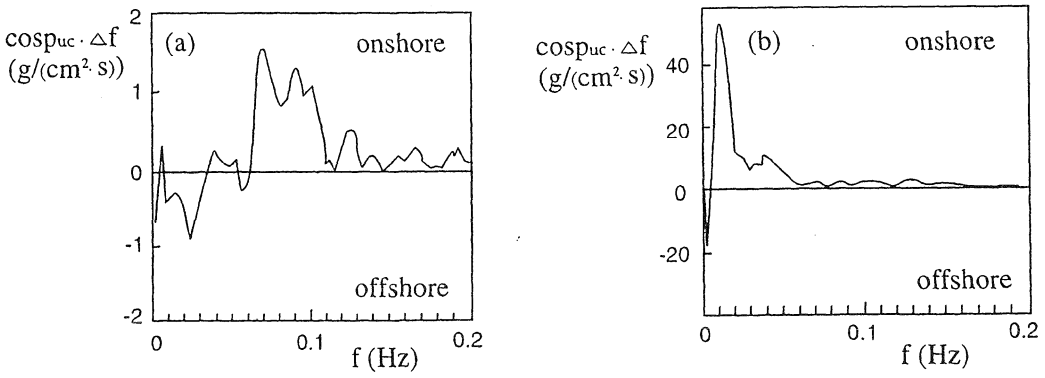

FIGURE 7.13. Cospectrum of u and c [5].

It is interesting that the phase-dependency of long waves on wave groupedness varies in the cross-shore direction, since the onshore transport due to long waves observed near the shoreline in Figures 7.11, 7.12, and 7.13b is considered to be associated with the phase-dependency. Sato and Mitsunobu [33] calculated the correlation coefficient C_{Hu} between the wave height H of short-wave component and the cross-shore velocity u_l of long-wave component through laboratory experiments as well as a numerical model. Figure 7.14 shows the cross-shore distribution of C_{Hu} for random waves breaking on a 1/20 slope. The circles denote the estimation based on laboratory measurements and the solid line denotes the correlation calculated by the numerical models described in the previous section. The correlation is negative in the offshore region, indicating that u_l is directed offshore under large waves, but changes to positive near the shoreline. The change in the sign of the correlation factor between the long-wave and the short-wave envelope in the surf zone was also described in Abdelrahman and Thornton [2] and Roelvink and Stive [31]. The reversal of the phase-dependency may be explained by the interaction between short waves and the currents induced by the long-wave component. Since the magnitude of long wave increases toward the shoreline and the celerity of short waves decreases toward the shoreline, the transformation of short waves near the shoreline will be more strongly influenced by the currents induced by long-wave components. Near the shoreline, it is thought that large waves are likely to ride on the following currents rather than on the opposing currents, thus resulting in the positive correlation between H and u_l. Owing to the positive correlation between H and u_l, onshore transport of sediment is considered to occur near the shoreline, where sediments are suspended under large waves when the velocity induced by long waves is shoreward. The onshore transport near the shoreline realized by the reversed phase-dependency is considered to exert strong influences on the berm formation frequently observed under random waves. It should be noted, however, that the phase-dependency and the contribution of long waves to sediment transport are highly variable in space on natural beaches, especially on beaches with multiple sand bars [1, 27].

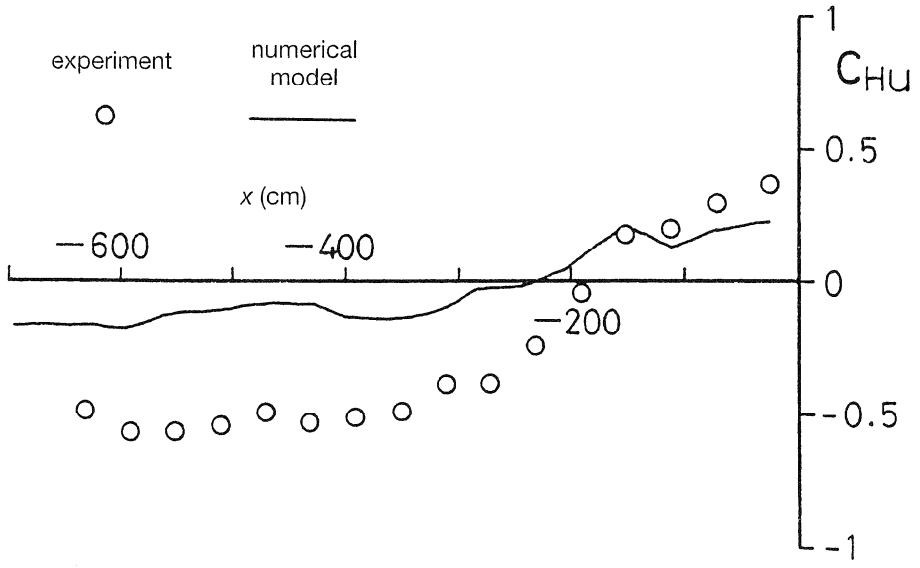

FIGURE 7.14. Correlation between short-wave height and velocity due to long-wave component [33].

4.4. Effect of Long Waves on Beach Profile Change

Effects of long waves on beach profile change have been studied through field investigations and laboratory experiments. In contrast to the accretive process suggested by the onshore transport near the shoreline described in the previous section, Katoh and Yanagishima [15] observed that berms were eroded by infragravity waves incident in the early stages of storms, as shown in Figure 7.15. Figure 7.15a shows the variation of offshore

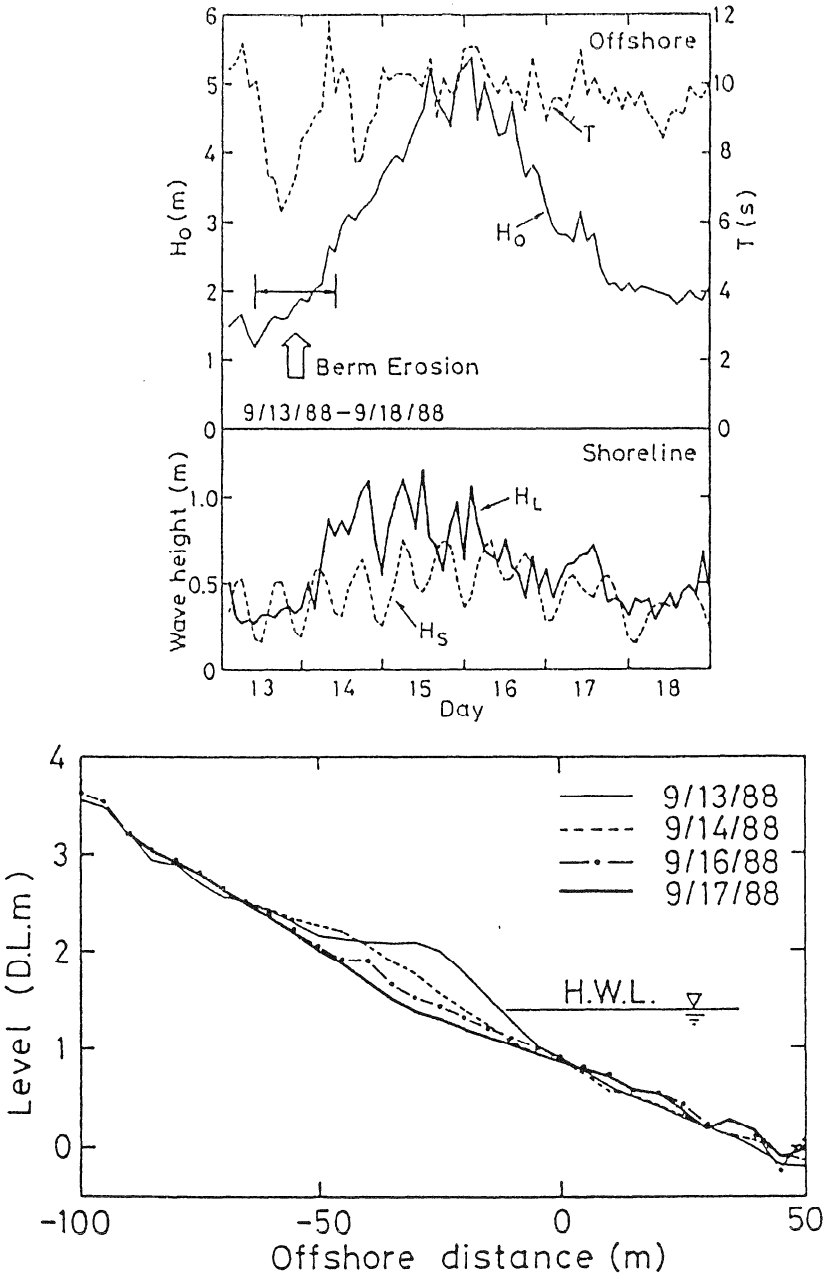

FIGURE 7.15. Berm erosion due to infragravity waves [15].

wave height H_0 and period T, as well as wave heights H_L of the long-wave component and H_S of the short-wave component observed near the shoreline. It is noticed that berm erosion occurred at the early stage of the storm, when the offshore waves were not well developed but significant long waves were incident on the beach. The difference between these conflicting results is considered to be due to the magnitude of the long-wave component. In Katoh and Yanagishima's [15] observation, the velocity due to long waves was very large near the shoreline, since observations were made when free long waves with large heights were incident prior to the storm, which flushed the berm away by large shear stress induced by long wave itself. In the mechanism described in the previous section, on the other hand, the role of long waves is secondary, transporting sand suspended by short waves.

Long waves are also considered to be associated with the formation of sand bars. Roelvink and Stive [31] showed by a numerical model and Dally [8] showed by laboratory experiments that the location of a sand bar was shifted when the development of long waves was suppressed. The relationship between standing long waves and the development of offshore bars was discussed in Short [38], Katoh [14], and Aagaard and Greenwood [1].

5. NUMERICAL MODELING OF BEACH PROFILE CHANGE

The numerical modeling of nearshore waves and the transformation of beach profiles is one of the most important subjects in the field of coastal engineering. Among various models presented so far, deterministic models, which are based on the modeling of physical processes in the surf zone, are promising since they have a potential ability to simulate dynamic beach evolution for a wide range of conditions. The deterministic models are mostly composed of the following submodels:

1. Wave transformation, including shoaling and breaking
2. Velocity field, especially near the bottom
3. Estimation of local sand transport rate
4. Bottom topography change based on mass conservation of sediments.

The change in beach profile will influence wave transformation, hence closed-loop iterations are required. In this section, the application of sand transport models under random waves will be described. The intercomparison of beach profiles predicted by various deterministic models was reviewed elsewhere [30].

Sato and Mitsunobu [33] tested the applicability of sediment transport formulas to random-wave conditions for four models—those proposed by Bailard [4], Sunamura [42], Shibayama and Horikawa [37], and Dibajnia and Watanabe [10]. The sediment transport formula proposed by Sunamura [42] was derived on the basis of laboratory measurements with monochromatic waves, and was expressed in terms of the Ursell parameter U_r and nondimensional velocity amplitude Ψ'' near the bottom, as follows:

$$U_r = \frac{gHT^2}{d^2}, \qquad \Psi'' = \frac{H^2}{sdD} \tag{17}$$

where H is the wave height, T the wave period, d the water depth, D the sediment diameter, and s the specific gravity of sand particles in water. The net sand transport rate was expressed by

$$\frac{Q}{w_s D} = \begin{cases} 0 & : \Psi'' \leq 17 \\ -3.00 \times 10^{-6} U_r (\Psi'' - 17)^2 & : \Psi'' > 17,\ U_r \leq 50 \\ -3.75 \times 10^{-1} U_r^{\ 2} (\Psi'' - 17)(\Psi'' - 0.048 U_r^{1.5}) & : \Psi'' > 17,\ 50 < U_r \leq 230 \\ -6.9 \times 10^{-8} U_r^{-0.2} \Psi''(\Psi'' - 0.13 U_r) & : \Psi'' > 17,\ U_r \geq 230 \end{cases} \tag{18}$$

where Q is the volumetric net sand transport rate and w_s the settling velocity of sand particles.

Dibajnia and Watanabe's [10] model is based on the assumption that the net sand transport rate is proportional to the product of excessive bottom shear stress and velocity amplitude. The net sand transport rate is expressed by a sum of wave-induced transport and turbulence-induced transport due to wave breaking, as follows:

$$\hat{u} = \frac{\pi H}{T \sinh kd'} \qquad \tau = \frac{1}{2} \rho f_w \hat{u}^2 \tag{19}$$

$$Q = \left(A_w \frac{\tau - \tau_c}{\rho g} \hat{u} + A_{wb} \frac{f_D E}{\rho g} \right) F_D \tag{20}$$

$$F_D = \tanh\left[\kappa_d \frac{(f_w \Pi)_c - f_w \Pi}{(f_w \Pi)_c} \right], \qquad \Pi = \frac{\hat{u}^2}{sgD} \frac{d}{L_0} \tag{21}$$

where τ is the bottom shear stress, f_w, the wave friction factor, τ_c the critical shear stress for the movement of sand particles, $\hat{u}$ the velocity amplitude, f_D the energy dissipation factor due to wave breaking, E the wave energy density, and F_D is a function that determines the direction of net sand transport. Both the Sunamura [42] and Dibajnia and Watanabe [10] models express net sand transport due to individual waves in terms of parameters of individual waves. In order to apply them to random waves, the total net sand transport rate is estimated by a sum of contributions separately calculated for individual waves. The estimation of the net sand transport rate under random waves by the superposition of individual wave contributions was also adopted by Larson [20] by using a different sand transport model.

Bailard's [4] model assumes that sand transport rates are expressed in terms of moments of near-bottom velocity. The net sand transport rates are expressed as a sum of bed load and suspended load, as follows:

$$Q = \frac{\overline{q(t)}}{(\rho_s - \rho) g} \tag{22}$$

$$q(t) = \rho C_f \frac{\epsilon_B}{\tan\phi} \left[u(t)|u(t)|^2 - \frac{\tan\beta}{\tan\phi} |u(t)|^3 \right] + \rho C_f \frac{\epsilon_S}{w_s} \left[u(t)|u(t)|^3 - \frac{\epsilon_S}{w_s} \tan\beta |u(t)|^5 \right] \tag{23}$$

where $q(t)$ is the instantaneous sand transport rate in immersed weight, C_f the drag coefficient, ϵ_B and ϵ_S coefficients for bed load, and suspended load respectively, tan ϕ the angle of repose of sand particles.

Shibayama and Horikawa's [37] model is based on the Shields parameter Ψ and the ratio $\hat{u}/w_s$ of velocity amplitude to settling velocity for a half wave cycle. The sand transport rate during the half wave cycle is expressed by the following formula, depending on sand transport types also categorized by Ψ and $\hat{u}/w_s$.

$$\frac{Q}{w_s D} = \begin{cases} 19\Psi^3 & : \text{bed load} \\ (1 - \alpha - N\alpha) 19\Psi^3 & : \text{bed load–suspended load transition} \\ -19N\Psi^3 & : \text{suspended load} \\ 19\Psi^3 & : \text{sheetflow} \end{cases} \tag{24}$$

where $N(=d_0/\lambda)$ is the ratio of orbital diameter d_0 of wave-induced particle motion near the bottom to the wavelength λ of sand ripples, and α is a parameter determined by Ψ and $\hat{u}/w_s$. Sato and Mitsunobu [33] modified the Shibayama and Horikawa [37] model, since their model predicted unrealistic change of Q when the transport type changed from suspended load to sheet flow. The modified sand transport rate in the transition region is expressed by

$$\frac{Q}{w_s D} = (1 - \Lambda)19\,\Psi^3 + \Lambda(-19N\Psi^3) \tag{25}$$

$$\Lambda = [1 - (\Psi_{rms}/0.6)^2] \times \min(1, 2/N) \tag{26}$$

where Ψ_{rms} is the Shields parameter based on the root-mean-square amplitude of velocity variation near the bottom.

In the Bailard [4] and Shibayama and Horikawa [37] models, net sand transport rates are estimated on the basis of velocity variation near the bottom. The direction and the amount of the net sand transport rates are therefore sensitive to the asymmetry in velocities discussed in the previous sections. A numerical model proposed by Sato and Mitsunobu [33], which simulated the wave height decay in the surf zone, the development of undertow, and the interaction of u_w and u_l under random waves, as described in the previous section, was applied to the estimation of cross-shore distribution of net sand transport rate under a random-wave condition on a uniform 1/20 slope, shown in Figure 7.16.

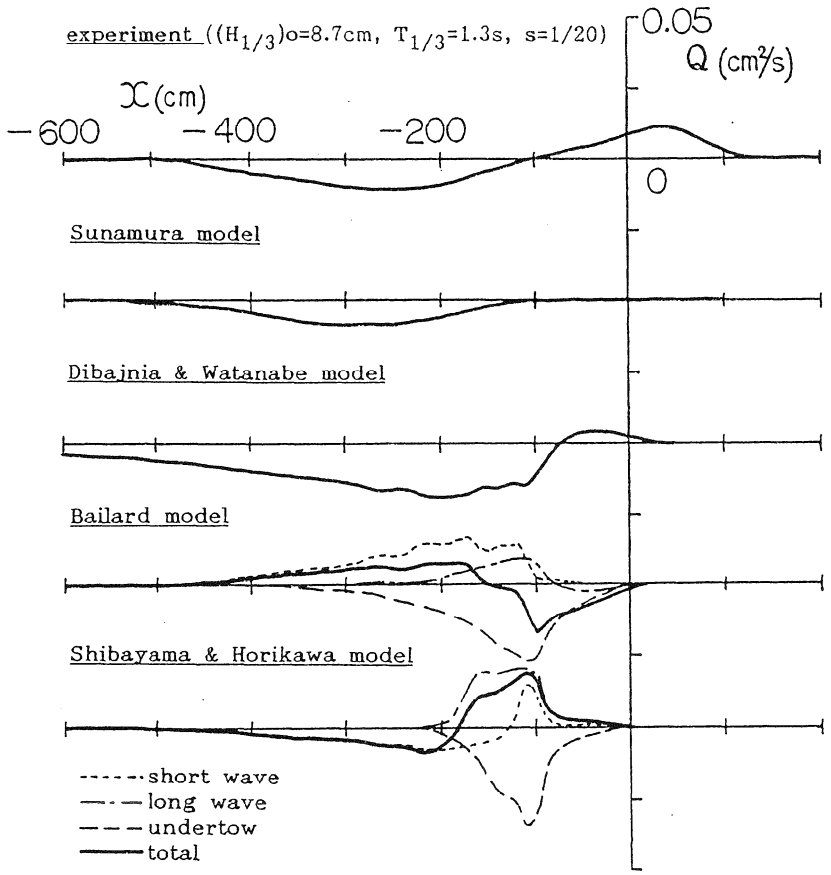

FIGURE 7.16. Cross-shore distributions of net sand transport rate [33].

On the top of Figure 7.16 is shown the net sand transport rate calculated from laboratory measurements [22]. It is noticed that seaward transport is dominant around the breaking point and shoreward transport is dominant near the swash zone. The resultant beach profile in this case is that of the intermediate type. In the offshore region, the Sunamura [42], Dibajnia and Watanabe [10], and Shibayama and Horikawa [37] models give similar seaward transport with slight differences in their magnitudes. The Bailard [4] model, however, predicts shoreward transport in the offshore zone. This is considered to be due to the energetic approach, which neglects the reverse transport of fine sand caused by vortices over sand ripples. Regarding surf zone transport, the Sunamura [42] model fails to estimate shoreward transport, but both the Dibajnia and Watanabe [10] and Shibayama and Horikawa [37] models predict shoreward transport, although the location of the maximum onshore transport is shifted to seaward.

Since the Bailard [4] and Shibayama and Horikawa [37] models are based on temporal variations of near-bottom velocities, it is interesting to identify contributions of various components. As the sand transport process is nonlinear, the contribution Q_l of the long-wave component is calculated, for example, by the following equation,

$$Q_l = Q(U + u_l + u_w) - Q_{l0}(U + u_w) \tag{27}$$

where Q_{l0} is the net sand transport rate computed by using velocity variations without long-wave components. It is noticed in Figure 7.16 that the steady component contributes to seaward transport and the long-wave component mainly to shoreward transport. The difference between these two models is primarily due to the difference in the short-wave contribution. It is interesting that the contribution by the long-wave component demonstrates similar distributions in both models. In order to determine the contribution of each component on natural beaches, further study is needed on the application of other sand transport models to random-wave conditions and on the comparison with large-scale random-wave experiments.

6. SUMMARY

Various models of beach transformation due to random waves were reviewed. They included simple parameter methods and sophisticated deterministic models composed of numerical submodels for waves, currents, and sediment movement. It was shown that deterministic models can simulate the beach profile change due to random waves provided that proper models are used in the estimation of the asymmetry in nonlinear wave orbital motion and undertow. The role of long waves in cross-shore sediment transport was also described.

Although deterministic models are still in the developing stage, they are promising, since the validity of the submodels can be checked and improved for each physical process. Among the physical processes that crucially affect sediment movement, sediment suspension due to wave breaking needs to be studied intensively in the near future in order to improve the estimation of the sand transport rate. It is stressed as a concluding remark that no numerical models can be developed without careful observations of the phenomena and informative data obtained in the experiments. Much attention should therefore be paid to measurements in laboratories and in the field to establish a rational beach evolution model.

REFERENCES

1. Aagaard, T. and B. Greenwood. 1994. Suspended sediment transport and the role of infragravity waves in a barred surf zone, *Marine Geology, 118,* 23–48.

2. Abdelrahman, S. M. and E. B. Thornton. 1987. Changes in the short wave amplitude and wavenumber due to the presence of infragravity waves, *Proceedings Specialty Conference on Coastal Hydrodynamics,* pp. 458–478.
3. Abbott, M. B. 1991, Numerical Modeling, in *Handbook of Coastal and Ocean Engineering,* ed. J. B. Herbich, Vol. 2, Gulf Publishing Company.
4. Bailard, J. A. 1982, Modeling on-offshore sediment transport in the surf zone, *Proceedings 18th Conference on Coastal Engineering,* ASCE, pp. 1419–1438.
5. Beach, R. A. and R. W. Sternberg. 1991. Infragravity driven suspended sediment transport in the swash, inner and outer-surf zone, *Coastal Sediments '91,* ASCE, pp. 114–128.
6. Bird, E. C. F. 1985. *Coastline Changes, A Global Review,* New York: Wiley, 219 pp.
7. Dally, W. R. and R. G. Dean. 1984., Suspended sediment transport and beach profile evolution, *J. Waterways, Port, Coastal and Ocean Engineering,* ASCE, Vol. 110, pp. 15–33.
8. Dally, W. R. 1991. Long wave effects in laboratory studies of cross-shore transport, *Coastal Sediments '91,* ASCE, pp. 85–99.
9. Dean, R. G. 1973. Heuristic models of sand transport in the surf zone, *Proceedings Conference on Engineering Dynamics in the Surf Zone,* ASCE, pp. 208–214.
10. Dibajnia, M. and A. Watanabe 1987. A numerical model of wave deformation and beach transformation in surf zone, *Proceedings 34th Japanese Conference on Coastal Engineering,* JSCE, pp. 291–295. (in Japanese)
11. Horikawa, K. 1978. *Coastal Engineering—An Introduction to Ocean Engineering,* University of Tokyo Press, 402 pp.
12. Iwagaki, Y. and H. Noda 1963. Laboratory study of scale effects in two-dimensional beach processes, *Proceedings 8th Conferenceon Coastal Engineering,* ASCE, pp. 194–210.
13. Johnson, J. W. 1949. Scale effects in hydraulic models involving wave motion, *Trans. A.G. U., 30*(4), 517–525.
14. Katoh, K. 1984. Multiple longshore bars formed by long period standing waves, *Rep. of Port and Harbour Res. Inst., 23*(3), 3–46.
15. Katoh, K. and S. Yanagishima. 1990. Berm erosion due to long period waves, *Proceedings 22nd Conference on Coastal Engineering,* ASCE, pp. 2073–2086.
16. Komar, P. D. 1976. *Beach Processes and Sedimentation,* Englewood Cliffs: Prentice-Hall, 429 pp.
17. Komar, P. D. 1991, Littoral sediment transport, in *Handbook of Coastal and Ocean Engineering,* ed. J. B. Herbich, Gulf Publishing Company, Vol.2, pp. 681–714.
18. Kraus, N. C., M. Larson, and D. L. Kriebel. 1991, Evaluation of beach erosion and accretion predictors, *Coastal Sediments '91,* ASCE, pp. 572–587.
19. Kriebel, D. L., W. R. Dally, and R. G. Dean. 1986. Undistorted Froude model for surf zone sediment transport, *Proceedings 20th Conference on Coastal Engineering,* ASCE, pp. 1296–1310.
20. Larson, M. 1994. Prediction of beach profile change at mesoscale under random waves, *Proceedings 24th Conference on Coastal Engineering,* ASCE, pp. 2252–2266.
21. Longuet-Higgins, M. S. and R. W. Stewart. 1962. Radiation stress and mass transport in gravity waves, with application to "surf beat," *J. Fluid Mech., 13,* 481–504.
22. Mimura N., Y. Ohtsuka, and A. Watanabe. 1986. Laboratory study on two-dimensional beach transformation due to irregular waves, *Proceedings 20th Conference on Coastal Engineering,* ASCE, pp. 1393–1406.
23. Mizuguchi, M. 1982. A field observation of wave kinematics in the surf zone, *Coastal Engineering in Japan,* Vol. 25, JSCE, pp. 91–107.
24. Nishimura, H. 1981. A model for rocky coast (I), NERC Report, No. 13. (in Japanese)
25. Okayasu, A., A. Watanabe, and M. Isobe. 1990. Modeling of energy transfer and undertow in the surf zone, *Proceedings 22nd Conference on Coastal Engineering,* ASCE, pp. 123–135.
26. Osborne, P. D. and B. Greenwood. 1992a. Frequency dependent cross-shore suspended sediment transport, 1. A non-barred shoreface, *Marine Geology, 106,* 1–24.
27. Osborne, P. D. and B. Greenwood 1992b, Frequency dependent cross-shore suspended sediment transport, 2. A barred shoreface, *Marine Geology, 106,* 25–51.
28. Ribberink, J. A. and A. A. Al-Salem. 1994. Sediment transport in oscillatory boundary layers in cases of rippled beds and sheetflow, *J. Geophys. Res., 99*(C6), 12707–12727.
29. Roelvink, J. A. 1993. Surf beat and its effect on cross-shore profiles, Ph.D Thesis, Delft University of Techology, 150 pp.

30. Roelvink, J. A. and I. Broker. 1993. Cross-shore profile models, *Coastal Engineering*, Elsevier, Vol. 21, pp. 163–191.
31. Roelvink, J. A. and M. J. F. Stive. 1989. Bar-generating cross-shore flow mechanisms on a beach, *J. Geophys. Res., 94*(C4), 4785–4800.
32. Sato, S. and K. Horikawa. 1986. Laboratory study on sand transport due to asymmetric oscillatory flows, *Proceedings 20th Conference on Coastal Engineering*, ASCE, pp. 1481–1495.
33. Sato, S. and N. Mitsunobu. 1991. A numerical model of beach profile change due to random waves, *Coastal Sediments '91*, ASCE, pp. 674–687.
34. Sato, S. and M. Kabiling. 1994. A numerical simulation of beach evolution based on a nonlinear dispersive wave-current model, *Proceedings 24th Conference on Coastal Engineering*, ASCE, pp. 2557–2570.
35. Saville, T., Jr. 1957. Scale effects in two-dimensional beach studies, *Proceedings 7th General Meeting*, IAHR, pp. 1–8.
36. Shi, N. C. and L. H. Larsen. 1984. Reverse sediment transport by amplitude-modulated waves, *Marine Geology, 54*, 181–200.
37. Shibayama, T. and K. Horikawa. 1985. A numerical model for two-dimensional beach transformation, *Proceedings JSCE*, Vol. 357/II-3, pp. 167–176.
38. Short, A. D. 1975. Multiple offshore bars and standing waves, *J. Geophys. Res., 80*(27), 3838–3840.
39. Southgate, H. N. and R. B. Nairn 1993. Deterministic profile modeling of nearshore processes. Part 1. Waves and Currents, *Coastal Engineering*, Elsevier, Vol. 19, pp. 27–56.
40. Stive, M. J. F. 1986. A model for cross-shore sediment transport, *Proceedings 20th Conference on Coastal Engineering*, ASCE, pp. 1550–1564.
41. Sunamura, T. and K. Horikawa. 1974. Two-dimensional beach transformation due to waves, *Proceedings 14th Conference on Coastal Engineering*, ASCE, pp. 920–938.
42. Sunamura, T. 1984. Prediction of on/offshore sediment transport rate in the surf zone including swash zone, *Proceedings 31st Japanese Conference on Coastal Engineering*, JSCE, pp. 316–320. (in Japanese)
43. Svendsen, I. A. 1984. Mass flux and undertow in a surf zone, *Coastal Engineering*, Elsevier, Vol. 8, pp. 347–365.
44. Symonds, G., D. A. Huntley, and A. J. Bowen 1982. Two-dimensional surf beat: Long wave generation by a time-varying breakpoint, *J. Geophys. Res., 87*(C1), 492–498.
45. Watanabe, A. and M. Dibajnia. 1988. Numerical modeling of nearshore waves, cross-shore sediment transport and beach profile change, *Proceedings IAHR Symp. on Mathematical Modeling of Sediment Transport in the Coastal Zone*, pp. 166–174.
46. Wright, L. D., J. D. Boon, S. C. Kim, and J. H. List. 1991. Modes of cross-shore sediment transport on the shoreface of the Middle Atlantic Bight, *Marine Geology, 96*, 19–51.
47. Wright, L. D., J. P. Xu, and O. S. Madsen. 1994. Across-shelf benthic transports on the inner shelf of the Middle Atlantic Bight during the "Halloween storm" of 1991, *Marine Geology, 118*, 61–77.